

Interaction Effects on the Electronic Floquet Spectra: Excitonic Effects

Teng Xiao,¹ Tsan Huang,¹ Changhua Bao,¹ and Zhiyuan Sun^{1,2,*}

¹State Key Laboratory of Low-Dimensional Quantum Physics and Department of Physics, Tsinghua University, Beijing 100084, P. R. China

²Frontier Science Center for Quantum Information, Beijing 100084, P. R. China

(Dated: June 9, 2025)

Floquet engineering of electronic states by light is a central topic in modern experiments. However, the impact of many-body interactions on the single-electron properties remains unclear in this non-equilibrium situation. We propose that interaction effects could be reasonably understood by performing perturbative expansion in both the pump field and the electron-electron interaction when computing physical quantities. As an example, we apply this approach to semiconductors and show analytically that excitonic effects, i.e., effects of electron-hole interaction, lead to dramatic corrections to the single-electron Floquet spectra even when the excitons are only virtually excited by the pump light. We compute these effects in phosphorene and monolayer MoS₂ for time- and angle-resolved photoemission spectroscopy (Tr-ARPES) and ultrafast optical experiments.

As a central arsenal of modern experiments, ultrafast lasers have been widely used to manipulate and explore the electronic properties in solid-state materials. When the laser pulse (the pump) is a multi-cycle one, the pumped material could be treated as a periodically driven system, giving rise to non-equilibrium states widely described in the language of Floquet engineering [1–5]. For example, the time- and angle-resolved photo-emission spectroscopy (Tr-ARPES) could generate the Floquet electronic states and directly probe their energy-momentum band dispersion [6–12]. On the other hand, the impact of many-body interactions on the Floquet electronic spectra is still in the mist [13–17]. The conventional theoretical approach computes the exact single-electron Floquet bands as the first step which typically has to be done numerically [18–21], and then performs perturbation in the electron-electron interaction on top of it. This method is limited by substantial numerical complexity and the lack of analytical clarity.

In this letter, we show that interaction effects in electronic Floquet bands could be understood analytically from a simpler approach, which performs perturbative expansion in both the pump field [22] and the electron-electron interaction. By deriving the dramatic excitonic and phononic corrections to the Floquet electronic bands in semiconductors, we show that this method enjoys both physical clarity and computational efficiency.

For example, when computing the electronic Green function (propagator)

$$G = \begin{pmatrix} G^R & G^K \\ 0 & G^A \end{pmatrix} = (G_0^{-1} - \Sigma)^{-1} \quad (1)$$

from the equilibrium bare Green function G_0 , the self-energy Σ could be perturbatively expanded in the driving field $E(t) = \int d\omega_p E(\omega_p) e^{-i\omega_p t}$ as shown by the red wavy lines in Fig. 1(b). In non-equilibrium systems, instead of imaginary-time Green functions, calculations should be performed in principle using real-time Green functions directly [23–27], for which the neatest notation is the two-by-two Green function in Eq. (1) that includes the retarded (G^R), advanced (G^A) and Keldysh (G^K) components introduced by Keldysh [24–27], see SI Sec. I for definitions. This Green function contains the

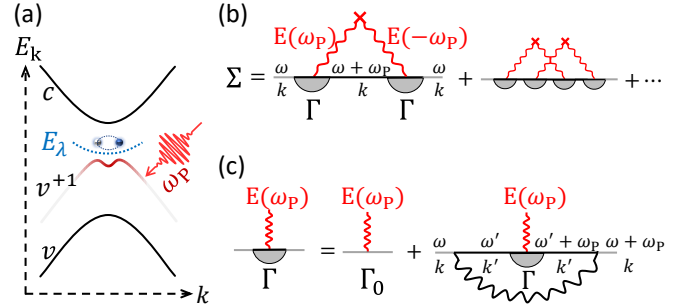


FIG. 1. (a) Schematic of a semiconductor with conduction band c and valence band v represented by black lines. Driven by pump light at frequency ω_p , the electron is virtually pumped to a Floquet side band $v+1$ (red curve) which is dramatically corrected by the virtual excitation of the zero momentum excitonic mode on the blue dashed curve. The (b-c) The Feynman diagrams of the self-energy Σ and the light-matter vertex Γ . The red wavy lines represent the electric field of the pump light connected in pairs to the ‘disorder’ vertices. The black wavy lines are the electron-hole interaction.

information of nearly all single particle properties such as the energy dispersion, occupation and spectral weight, and is the central quantity in this paper.

The Green function $G(t_0 + t/2, t_0 - t/2)$ could be written in the frequency representation as $G(\omega, t_0) = \int_{-\infty}^{\infty} dt e^{i\omega t} G(t_0 + t/2, t_0 - t/2)$ which is not time-translational invariant. Since G typically depends on the central time t_0 in a fast oscillating manner during the pump pulse which can hardly be resolved in ultrafast experiments, we focus on its time-averaged component $G(\omega) = \int_0^T G(\omega, t_0) dt_0 / T$ where T is a time scale much larger than the typical period of the pump light. It reduces to the equilibrium Green function in the limit of zero driving field. If one puts it in the context of the Green function $G_{m,n}(\omega)$ of a strictly periodically driven system where m, n are integers [28], the Green function used here is $G(\omega) = G_{0,0}(\omega)$. However, note that our approach is not limited to periodically driven systems and could also deal with the case of ultrafast pump, i.e., when the frequency spectra $E(\omega_p)$ is not a delta function.

For the Green function of interest, the perturbative expansion of the self-energy Σ in the pump field is similar to that for the disorder potential, see Fig. 1(b). It contains every diagram that satisfies two conditions: 1, it is one-particle-irreducible (1PI) meaning that it cannot be separated by cutting a electron propagator with the frequency labeling ω ; 2, there are equal numbers of lines of the driving field E at the frequencies ω_p and $-\omega_p$ so that the self energy does not change the frequency. Every pair of driving field lines connected to the same ‘disorder’ vertex gives a Gaussian-ensemble-averaged driving power: $\langle E(\omega_p)E(\omega'_p) \rangle = S(\omega_p)\delta(\omega_p - \omega'_p)$, which applies to the case when the pump pulse has random phases. The lowest order self energy is therefore

$$\Sigma = \int d\omega_p \Gamma(-\omega_p) G_0(\omega + \omega_p) \Gamma(\omega_p) \quad (2)$$

as shown by the first diagram in Fig. 1(b) where Γ is the electron-photon vertex shown in Fig. 1(c). The Dyson’s equation (Eq. (1)) yields a Green function to infinite order in Σ . Perturbation in electron-electron, electron-phonon or electron-impurity interactions could be added diagrammatically in similar ways to the equilibrium situation, e.g., as corrections to the vertex Γ or to the bare Green function G_0 . For materials driven by light, the most dramatic effect occurs when an optically active collective mode, such as an infrared phonon or exciton that couples to the electrons, is driven linearly by light. This effect is contained in the interaction correction to the electron-photon vertex Γ , as shown by Fig. 1(c) for the case of excitonic correction, i.e., correction from electron-hole interaction.

Excitonic corrections—We now apply this method to compute the excitonic correction to the Floquet electronic bands in semiconductors driven by light. We show analytically that the optically active excitonic modes lead to dramatic corrections to both the energy and occupation of the bands. Predictions are shown for monolayer black phosphorus (phosphorene) and monolayer MoS₂ to be verified by Tr-ARPES or ultrafast optical experiments. We note that although people have tried to calculate the Tr-ARPES signatures of excitons with numerical methods [29–35], this work provides a unified analytical method that offers physical understanding.

A minimal two band Hamiltonian for semiconductors with electron-hole interaction and nonzero interband optical matrix element is

$$H = \sum_k \begin{pmatrix} c_k \\ v_k \end{pmatrix}^\dagger \begin{pmatrix} \varepsilon_{k+A}^c & A \cdot M_k \\ A \cdot M_k^* & \varepsilon_{k+A}^v \end{pmatrix} \begin{pmatrix} c_k \\ v_k \end{pmatrix} + H_{ee}, \quad (3)$$

$$H_{ee} = \sum_{k,k',q} V_q v_{k'-q}^\dagger v_{k'} c_{k+q}^\dagger c_k$$

where $\varepsilon_k^v = -k^2/2m_v$ ($\varepsilon_k^c = E_g + k^2/2m_c$) is the kinetic energy of the valence (conduction) band electrons whose annihilation operators are v_k (c_k) at momentum k , $E_g > 0$ is the band gap, and V_q is the density-density interaction kernel between electrons of the two bands. For notational simplicity,

we set the Planck constant \hbar , the elementary charge e and the speed of light c to be 1.

For clear illustration of the physics, we use the single color pump light with the electric field $E = -\partial_t A$ represented by the vector potential $A(t) = A_0 e^{-i\omega_p t} + \text{c.c.}$ so that one does not need to perform the integral in ω_p in Eq. (2). The vector potential couples to electrons through the Peierls substitution and the interband optical matrix element $A_0 M_k = iE_0 M_k / \omega_p$ so that Eq. (3) is not manifestly gauge invariant.

From single particle analysis neglecting H_{ee} , as the driving field is turned on, the electronic bands become Floquet bands (contained in the poles of the Green function), such as the v^{+1} band shown in Fig. 1(a). Taking into account the electron-hole attraction H_{ee} , there are electron-hole bound state excitations within the gap in the excitation spectrum: the bosonic excitations called excitons. Since the pump light couples to the interband transition terms through M_k , it could linearly drive the excitonic excitations in the same way as driving harmonic oscillators. More interestingly, when the pump frequency ω_p is close to an exciton resonance, the forced excitonic oscillation is resonantly enhanced, so that one expects dramatic interaction corrections to the electronic Floquet bands.

We now calculate this excitonic correction analytically, which is contained in the interaction modified vertex Γ_k shown in Fig. 1(c). Summing the ladder diagrams renders

$$\Gamma_k^{cv}(\omega_p) = A_0 \sum_\lambda C_\lambda \frac{\omega_p + \varepsilon_k^v - \varepsilon_k^c + i0^+}{\omega_p - \omega_\lambda + i\gamma_\lambda} \phi_\lambda(k) \quad (4)$$

where λ labels the electron-hole two-body eigen state $\phi_\lambda(k)$ with the eigen energy ω_λ satisfying the Wannier equation

$$(\varepsilon_k^c - \varepsilon_k^v - \omega_\lambda) \phi_\lambda(k) = \sum_{k'} V_{k-k'} \phi_\lambda(k'), \quad (5)$$

see SI Sec. II. The coefficient $C_\lambda = \sum_{k'} M_{k'} \phi_\lambda^*(k')$ is the overlap between the interband optical matrix element and $\phi_\lambda(k)$. The pole structure in Eq. (4) comes from the retarded Green function of the excitons, to which we have added the phenomenological damping rate γ_λ . Note the index λ contains both the bound and scattering states while only bound states with $\omega_\lambda < E_g$ correspond to excitons. Plugging Eq. (4) (and Γ^{vc} , Γ^{cc} , Γ^{vv}) into Eqs. (2) and (1) yields the electronic self energy and Green function. The poles of the latter give the energies of the Floquet bands.

To make connections to the conventional single particle approach to Floquet bands, the vertex is an energy scale that hybridizes the corresponding bare Floquet replica of the bands. The interaction corrected Floquet bands are the same as those from diagonalizing the Floquet Hamiltonian (with a cutoff of $\pm\omega_p$) from Eq. (3) without H_{ee} , but with the interband optical matrix element AM_k (AM_k^*) replaced by the interaction-corrected vertex Γ_k^{cv} (Γ_k^{vc}), see SI Sec. V.

The physical consequence is more transparent if the pump frequency ω_p is close to the eigen energy ω_λ of a certain exci-

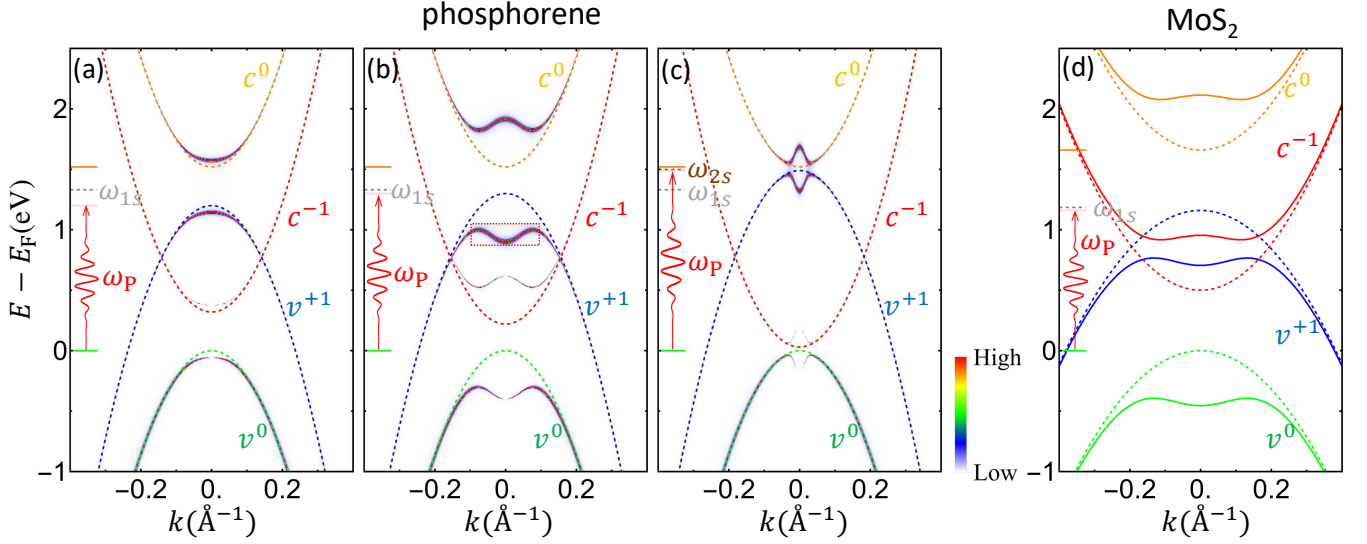


FIG. 2. (a,b,c) Floquet electronic spectra of phosphorene driven by pump light at frequencies $\omega_P = 1.200$ eV, 1.300 eV, 1.490 eV, respectively. The colored dashed curves labeled by c^0 , c^{-1} , v^{+1} , and v^0 are the four low energy Floquet electronic bands predicted by free theory without interaction corrections. The color map shows the photo emission intensity of the interaction corrected Floquet bands. The equilibrium conduction band minimum (valence band maximum) is indicated by the orange (green) horizontal line. The gray dashed line marks the energy of the $1s$ exciton ($E_{1s} = 1.331$ eV). The brown dashed line in (c) marks the energy of the $2s$ exciton ($E_{2s} = 1.499$ eV). Here, $m_c = 0.17m_e$, $m_v = 0.18m_e$, $E_g = 1.52$ eV, $\epsilon = 5$, $\gamma_{1s} = \gamma_{2s} = 5$ meV, and $M_k = i5.25$ eVÅ [36]. The pump electric field is $E_0 = 5 \times 10^5$ V/cm and along the armchair (x) direction of phosphorene. The probe matrix elements are constrained by the symmetry of phosphorene: $M_{fc} = b_1$ and $M_{fv} = -b_1 M_k k / E_g$ where we set $b_1 = 1$, the probe incident plane is $z - y$ plane and the probe field is in the zigzag (y) direction [37]. (d) Similar to (a,b,c) but for the lowest conduction band and highest valence band of monolayer 1H MoS₂ with momenta measured from the K point. The Floquet bands with excitonic corrections are shown by solid lines instead. The parameters are $m_c = 0.40m_e$, $m_v = 0.48m_e$, $E_g = 1.66$ eV, $\epsilon = 5$, $E_{1s} = 1.18$ eV, $\gamma_{1s} = \gamma_{2s} = 1$ meV, $M_k = 3.51$ eVÅ, $\omega_P = 1.16$ eV and $E_0 = 2.9 \times 10^5$ V/cm.

ton. Here the vertex will be dominated by this exciton:

$$\Gamma_k^{cv}(\omega_P) \approx A_0 M \frac{\omega_P + \varepsilon_k^v - \varepsilon_k^c}{\omega_P - \omega_\lambda + i\gamma_\lambda} \phi_\lambda^*(r=0) \phi_\lambda(k) \equiv \Delta_k \quad (6)$$

where we assumed that $M_k = M$ so that the overlap coefficient becomes $C_\lambda = M \phi_\lambda^*(r=0)$ and that Δ_k is proportional to $\phi_\lambda(r=0)$, the probability amplitude that the electron and hole make a contact within the bound state. Physically, the local interband optical matrix element means that light excites the exciton by generating an electron and a hole at the same space location. From the poles of the retarded Green function G^R , the energy dispersion of the Floquet electronic bands are

$$E_{1/2}^c = \frac{\varepsilon_k^c + \varepsilon_k^v + \omega_P \pm \sqrt{(\varepsilon_k^c - \varepsilon_k^v - \omega_P)^2 + 4|\Delta_k|^2}}{2}, \quad (7)$$

$$E_{1/2}^v = \frac{\varepsilon_k^v + \varepsilon_k^c - \omega_P \pm \sqrt{(\varepsilon_k^v - \varepsilon_k^c + \omega_P)^2 + 4|\Delta_k|^2}}{2}$$

where $E_{1/2}^c$ are the two bands from the conduction band ε^c and the first Floquet replica (v^{+1}) of the valence band $\varepsilon^v + \omega_P$ after hybridizing with the matrix element Δ_k . Since Δ_k becomes large as the driving frequency ω_P is tuned close to ω_λ , the excitonic effect leads to dramatic corrections to the energy compared to the case without electron-hole interaction, as shown schematically in Fig. 1(a). According to Eq. (6),

the energy distortion as a function of momentum also reflects the electron-hole bound state wavefunction $\phi_\lambda(k)$. Similar effects occur for $E_{1/2}^v$, the hybridized bands from ε_k^v and $\varepsilon_k^c - \omega_P$ through Δ_k . Note that as ω_P approaches ω_λ , the vertex in Eq. (6) appears divergent if there is no excitonic damping. In fact, the large oscillation amplitude of the excitonic mode must cause a blue shift of the exciton energy via the exciton-exciton interaction [38, 39] so that the divergence is cured. This effect is contained in the pump induced corrections to the electron-photon vertex, which we address in future research.

The occupation information of the Floquet electronic bands could be found from the lesser Green function $G_{\alpha,\beta}^<(t_1, t_2) = i\langle \alpha^\dagger(t_2) \beta(t_1) \rangle = (G^K + G^A - G^R)/2$ where α, β takes values in $\{c, v\}$. For the v^{+1} pole shown in the Fig. 1(a), we obtain

$$G_{v^{+1}}^<(\omega) = 2\pi i \frac{|\Delta_k|^2}{(\varepsilon_k^c - \varepsilon_k^v - \omega_P)^2 + 4|\Delta_k|^2} \delta(\omega - E_2^c), \quad (8)$$

see SI Sec. IV. It is obvious that the occupation grows with Δ_k , i.e., the driving strength and the magnitude of the exciton wave function.

Phosphorene and MoS₂—To make quantitative predictions for experiments, we present in Fig. 2 the numerical results of phosphorene and monolayer MoS₂ using the two-band model in Eq. (3) with the parameters from their relevant bands. The energy dispersion of the Floquet bands are obtained by the

poles of the Green function from solving Eqs. (1)(2)(4)(5).

For the excitons, we use the two-dimensional Coulomb attraction with the kernel $V_q = 2\pi/(\epsilon q)$ in Eq. (5) where ϵ is the dielectric constant of the three-dimensional environment. It yields a Hydrogenic series of bound states [40]. For example, the 1s-exciton has the wave function $\phi_{1s}(k) = \sqrt{8\pi}q_0^2/(q_0^2 + k^2)^{3/2}$ and the binding energy $E_b = me^4/(\hbar^2\epsilon^2)$, where $q_0 = 2/a_0$, $a_0 = 2\epsilon\hbar^2/me^2$ is the exciton Bohr radius and $m = 2/(1/m_c + 1/m_v)$ is the reduced mass. We note that while two-dimensional screening from the monolayer itself changes the Coulomb attraction kernel to the Rytova-Keldysh potential [41], it doesn't bring qualitative changes to the picture [42–44], see the SI of Ref. [39].

A typical experiment to measure these Floquet bands is Tr-ARPES that probes the photoemission intensity [37]

$$I_k(\varepsilon_k^f) = -i|A_b|^2 \sum_{\alpha,\beta} M_{f\alpha}(k) M_{\beta f}(k) G_{\alpha\beta}^<(\varepsilon_k^f - \omega_b), \quad (9)$$

see SI Sec. VI. Here the vector potential of the probe field is $A_b(t) = A_b e^{-i\omega_b t} + \text{c.c.}$, M_{fc} (M_{fv}) is the optical matrix element between free electrons f and the electrons in conduction (valance) band, ε_k^f is the kinetic energy of the emitted free electron, and $G^<$ is the lesser Green function from Eq. (1) that contains the effect of the interaction and the pumping field.

In Fig. 2(a)(b)(c), we show the electronic energy dispersion of phosphorene under the pump light at three different frequencies. The dashed lines are the dispersion of the Floquet bands from free theory (without the H_{ee}), while the color scale shows the Tr-ARPES intensity $I_k(\omega + \omega_b)$ from Eq. (9) using the excitonic corrected Green functions. Compared to the free theory, the excitonic correction leads to dramatic downward bending of the v^{+1} band (e.g., in the region enclosed by the red dotted rectangle in Fig. 2(b)) and similar distortion for other bands. The shape of bending is *not* from a simple band crossing between the bare c^0 and v^{+1} bands because they haven't crossed each other before being hybridized by the optical vertex Δ_k in Eq. (6). Instead, it comes from the strong momentum dependence of the exciton wave function $\phi_{1s}(k)$ within the momentum range set by q_0 , the size of the exciton wave function, which is understood analytically from Eq. (7). In the same momentum range, the photo-emission intensity of the v^{+1} and c^0 bands are also greatly enhanced, reflecting the exciton-enhanced occupation number predicted by Eq. (8). In Fig. 2(c), we tune the pump frequency close to the 2s exciton so that the shape of bending highlights the exciton wave function $\phi_{2s}(k)$ with a momentum range of about $q_0/3$.

The v^{+1} band could also be understood as the ARPES signal of the virtual 1s excitons excited by the pump. However, we emphasize that the 1s exciton is only virtually excited by the pump light, in the same sense as a harmonic oscillator driven off resonance, different from the situation studied before [29–33]. Resonant excitation of the excitons is not required, and the excitonic correction to the electronic Floquet spectra exists at every driving frequency. For instance, if the driving frequency ω_p is shifted, the v^{+1} band, stemming from the replica of the valence band, shifts with it, as shown clearly

by Eq. (7). Therefore, our approach provides a unified analytical understanding of previous numerical results [29–34]. We note that exciton-Floquet effects under resonant pumping have been observed in a recent experiment [45], while the nontrivial excitonic corrections under off-resonant pump remains to be discovered using stronger pump and higher energy resolution.

Optically active Phonons—We now discuss a rather trivial example of collective mode correction to the electronic Floquet spectra in materials driven by light: the case of optically active phonons (often called ‘infrared phonons’) coupled to electrons. For the two-band semiconductor described by Eq. (3), the additional Hamiltonian describing the infrared phonon and its coupling to electrons and to light reads

$$H_{ep} = \omega_0 a^\dagger a + D (a + a^\dagger) E(t) + (a + a^\dagger) \sum_k \begin{pmatrix} c_k \\ v_k \end{pmatrix}^\dagger \begin{pmatrix} B_k^{cc} & B_k^{cv} \\ B_k^{vc} & B_k^{vv} \end{pmatrix} \begin{pmatrix} c_k \\ v_k \end{pmatrix} \quad (10)$$

where a (a^\dagger) is the annihilation (creation) operator for the zero-momentum infrared phonon with the intrinsic frequency ω_0 , B_k is the electron-phonon coupling matrix element, and D is the linear coupling matrix element between the phonon and the electric field.

The phonon is driven linearly by the pump light, thus modifying the electronic spectra by contributing a vertex as another correction to the vertex in Fig. 1(c). For instance, its interband component reads

$$\Gamma_p^{cv}(\omega_p) = E(\omega_p) B_k^{cv} D \frac{2\omega_0}{\omega_p^2 - \omega_0^2 + i\gamma\omega_p} \quad (11)$$

where the last term comes from the retarded response function of the phonon and we have added a phenomenological damping rate γ to it. For a single color drive, Eq. (11) should be simply added to Eq. (4) to yield the total vertex that corrects the band in Eq. (7). Apparently, when the pump frequency is close to the intrinsic phonon frequency, the driven phonon oscillation is resonantly enhanced and so is the phonon mediated correction to the electronic band. We note that the existence of an optically active phonon or exciton leads to a nontrivial dielectric function $\epsilon(\omega)$ of the solid that has resonant structures close to their frequencies. The electric field in Eqs. (3)(10) should be understood not as the external electric field, but as the total electric field after the screening effect which makes a big difference in three-dimensional materials.

Discussion—Before conclusion, we discuss the logic behind the re-summation in the driving field E_0 for the periodically driven case where $E(t) = E_0(e^{-i\omega_p t} + \text{c.c.})$. The Taylor expansion $G = \sum_n g_{2n} E_0^{2n}$ of the Green function in E_0 is re-summed by the Dyson equation in Eq. (1) so that one just needs to compute the self energy $\Sigma = \sum_n c_{2n} E^{2n}$. This is a common practice which assumes that among all the contributions to the coefficient g_{2n} , the irreducible diagrams are less important. The general argument for it is that in g_{2n} , the irreducible diagrams involve electron propagators at higher frequencies $(\omega + n\omega_p)$, which are small if one concerns

the low energy behavior of the Green function. Additionally, consider g_4 for the excitonic effects as an example, one is concerned with the case when ω_p is close to an exciton resonance so that the vertex $\Gamma^{cv}(\omega_p) = \Gamma^{vc}(-\omega_p) \sim 1/(\omega_p - \omega_\lambda)$ in Eq. (4) is large. Compared to the reducible diagram $G_0 \Sigma G_0 \Sigma G_0$ included by the Dyson's equation with the leading order self energy, the second diagram in Fig. 1(b) is smaller by the ratio $a_1 \sim \Gamma^{cv}(-\omega_p) G_0(\omega + 2\omega_p) \Gamma^{vc}(\omega_p) / [\Gamma^{cv}(\omega_p) G_0(\omega) \Gamma^{vc}(-\omega_p)] \sim (\omega_p - \omega_\lambda)^2 / (\omega_p - E_g)^2 \ll 1$ which is indeed a small parameter, see SI Sec. III.

With this perturbative approach, more interesting interaction effects are to be discovered for the Floquet electronic spectra, such as polaron effects and effects of collective modes in systems with charge/spin/excitonic orders. Given improved energy resolution in the pump and probe, we expect these intriguing phenomena to be observed by Tr-ARPES [45, 46] and ultrafast optical experiments [47, 48] in the near future.

This work is supported by the National Key Research and Development Program of China (2022YFA1204700), the National Natural Science Foundation of China (Grants No. 12374291 and No. 12421004), and the startup grant from Tsinghua University. We thank S. Zhou, J. Li and X. Yang for helpful discussions.

* zysun@tsinghua.edu.cn

- [1] T. Oka and S. Kitamura, Floquet Engineering of Quantum Materials, *Annu. Rev. Condens. Matter Phys.* **10**, 387 (2019).
- [2] M. S. Rudner and N. H. Lindner, Band structure engineering and non-equilibrium dynamics in Floquet topological insulators, *Nat. Rev. Phys.* **2**, 229 (2020).
- [3] A. de la Torre, D. M. Kennes, M. Claassen, S. Gerber, J. W. McIver, and M. A. Sentef, Colloquium: Nonthermal pathways to ultrafast control in quantum materials, *Rev. Mod. Phys.* **93**, 041002 (2021).
- [4] C. Bao, P. Tang, D. Sun, and S. Zhou, Light-induced emergent phenomena in 2D materials and topological materials, *Nat. Rev. Phys.* **4**, 33 (2022).
- [5] T. Oka and H. Aoki, Photovoltaic Hall effect in graphene, *Phys. Rev. B* **79**, 081406 (2009).
- [6] F. Boschini, M. Zonno, and A. Damascelli, Time-resolved ARPES studies of quantum materials, *Rev. Mod. Phys.* **96**, 015003 (2024).
- [7] Y. H. Wang, H. Steinberg, P. Jarillo-Herrero, and N. Gedik, Observation of Floquet-Bloch States on the Surface of a Topological Insulator, *Science* **342**, 453 (2013).
- [8] F. Mahmood, C.-K. Chan, Z. Alpichshev, D. Gardner, Y. Lee, P. A. Lee, and N. Gedik, Selective scattering between Floquet-Bloch and Volkov states in a topological insulator, *Nat. Phys.* **12**, 306 (2016).
- [9] S. Aeschlimann, S. A. Sato, R. Krause, M. Chávez-Cervantes, U. De Giovannini, H. Hübener, S. Forti, C. Coletti, K. Hanff, K. Rossnagel, A. Rubio, and I. Gierz, Survival of Floquet-Bloch States in the Presence of Scattering, *Nano Lett.* **21**, 5028 (2021).
- [10] S. Zhou, C. Bao, B. Fan, H. Zhou, Q. Gao, H. Zhong, T. Lin, H. Liu, P. Yu, P. Tang, S. Meng, W. Duan, and S. Zhou, Pseudospin-selective Floquet band engineering in black phosphorus, *Nature* **614**, 75 (2023).
- [11] S. Ito, M. Schüler, M. Meierhofer, S. Schlauderer, J. Freudenstein, J. Reimann, D. Afanasiev, K. A. Kokh, O. E. Tereshchenko, J. Gütde, M. A. Sentef, U. Höfer, and R. Huber, Build-up and dephasing of Floquet-Bloch bands on subcycle timescales, *Nature* **616**, 696 (2023).
- [12] S. Zhou, C. Bao, B. Fan, F. Wang, H. Zhong, H. Zhang, P. Tang, W. Duan, and S. Zhou, Floquet Engineering of Black Phosphorus upon Below-Gap Pumping, *Phys. Rev. Lett.* **131**, 116401 (2023).
- [13] M. Bukov, S. Gopalakrishnan, M. Knap, and E. Demler, Prethermal Floquet Steady States and Instabilities in the Periodically Driven, Weakly Interacting Bose-Hubbard Model, *Phys. Rev. Lett.* **115**, 205301 (2015).
- [14] D. M. Kennes, A. de la Torre, A. Ron, D. Hsieh, and A. J. Millis, Floquet Engineering in Quantum Chains, *Phys. Rev. Lett.* **120**, 127601 (2018).
- [15] M. Claassen, H.-C. Jiang, B. Moritz, and T. P. Devereaux, Dynamical time-reversal symmetry breaking and photo-induced chiral spin liquids in frustrated Mott insulators, *Nat. Commun.* **8**, 1192 (2017).
- [16] Y. Wang, C.-C. Chen, B. Moritz, and T. P. Devereaux, Light-Enhanced Spin Fluctuations and d -Wave Superconductivity at a Phase Boundary, *Phys. Rev. Lett.* **120**, 246402 (2018).
- [17] C. Xie, A. D. Smith, H. Yan, W.-C. Chen, and Y. Wang, Dynamical Approach to Realize Room-Temperature Superconductivity in LaH₁₀, *arXiv*: **2312**, 12706 (2023).
- [18] M. A. Sentef, M. Claassen, A. F. Kemper, B. Moritz, T. Oka, J. K. Freericks, and T. P. Devereaux, Theory of Floquet band formation and local pseudospin textures in pump-probe photoemission of graphene, *Nat. Commun.* **6**, 7047 (2015).
- [19] M. Schüler, D. Golež, Y. Murakami, N. Bittner, A. Herrmann, H. U. Strand, P. Werner, and M. Eckstein, Nessi: The non-equilibrium systems simulation package, *Computer Physics Communications* **257**, 107484 (2020).
- [20] X. Liu, B. Fan, H. Hübener, U. De Giovannini, W. Duan, A. Rubio, and P. Tang, Floquet engineering of magnetism in topological insulator thin films, *Electronic Structure* **5**, 024002 (2023).
- [21] H. Cao, J.-T. Sun, and S. Meng, Floquet engineering of anomalous Hall effects in monolayer MoS₂, *npj Quantum Mater.* **9**, 90 (2024).
- [22] Z. Sun, Floquet engineering of many-body states by the ponderomotive potential, *Phys. Rev. B* **110**, 104301 (2024).
- [23] L. P. Kadanoff and G. Baym, *Quantum Statistical Mechanics: Green's Function Methods in Equilibrium and Nonequilibrium Problems* (W.A. Benjamin, New York, 1962).
- [24] L. V. Keldysh, Diagram technique for nonequilibrium processes, *Zh. Eksp. Teor. Fiz.* **47**, 1515 (1964).
- [25] A. Kamenev, *Field Theory of Non-Equilibrium Systems* (Cambridge University Press, Cambridge, England, 2011).
- [26] A. Altland and B. Simons, *Condensed Matter Field Theory*, 3rd ed. (Cambridge University Press, Cambridge, England, 2023).
- [27] L. M. Sieberer, M. Buchhold, and S. Diehl, Keldysh field theory for driven open quantum systems, *Rep. Prog. Phys.* **79**, 096001 (2016).
- [28] H. Aoki, N. Tsuji, M. Eckstein, M. Kollar, T. Oka, and P. Werner, Nonequilibrium dynamical mean-field theory and its applications, *Rev. Mod. Phys.* **86**, 779 (2014).
- [29] E. Perfetto, D. Sangalli, A. Marini, and G. Stefanucci, First-principles approach to excitons in time-resolved and angle-resolved photoemission spectra, *Phys. Rev. B* **94**, 245303 (2016).
- [30] A. Rustagi and A. F. Kemper, Photoemission signature of exci-

- tons, *Phys. Rev. B* **97**, 235310 (2018).
- [31] D. Christiansen, M. Selig, E. Malic, R. Ernstorfer, and A. Knorr, Theory of exciton dynamics in time-resolved ARPES: Intra- and intervalley scattering in two-dimensional semiconductors, *Phys. Rev. B* **100**, 205401 (2019).
- [32] E. Peretto, D. Sangalli, A. Marini, and G. Stefanucci, Pump-driven normal-to-excitonic insulator transition: Josephson oscillations and signatures of BEC-BCS crossover in time-resolved ARPES, *Phys. Rev. Mater.* **3**, 124601 (2019).
- [33] Y.-H. Chan, D. Y. Qiu, F. H. da Jornada, and S. G. Louie, Giant self-driven exciton-Floquet signatures in time-resolved photoemission spectroscopy of MoS₂ from time-dependent GW approach, *Proc. Natl. Acad. Sci.* **120**, e2301957120 (2023).
- [34] H. Park, N. Park, and J. Lee, Novel Quantum States of Exciton-Floquet Composites: Electron-Hole Entanglement and Information, *Nano Lett.* **24**, 13192 (2024).
- [35] S. Beaulieu, S. Dong, V. Christiansson, P. Werner, T. Pincelli, J. D. Ziegler, T. Taniguchi, K. Watanabe, A. Chernikov, M. Wolf, L. Rettig, R. Ernstorfer, and M. Schüler, Berry curvature signatures in chiroptical excitonic transitions, *Science Advances* **10**, eadk3897 (2024).
- [36] J. M. Pereira and M. I. Katsnelson, Landau levels of single-layer and bilayer phosphorene, *Phys. Rev. B* **92**, 075437 (2015).
- [37] C. Bao, M. Schüler, T. Xiao, F. Wang, H. Zhong, T. Lin, X. Cai, T. Sheng, X. Tang, H. Zhang, P. Yu, Z. Sun, W. Duan, and S. Zhou, Manipulating the symmetry of photon-dressed electronic states, *Nat. Commun.* **15**, 10535 (2024).
- [38] F. C. Wu, F. Xue, and A. H. MacDonald, Theory of two-dimensional spatially indirect equilibrium exciton condensates, *Physical Review B* **92**, 165121 (2015).
- [39] Z. Sun, Y. Murakami, F. Xuan, T. Kaneko, D. Golež, and A. J. Millis, Dynamical Exciton Condensates in Biased Electron-Hole Bilayers, *Phys. Rev. Lett.* **133**, 217002 (2024).
- [40] X. L. Yang, S. H. Guo, F. T. Chan, K. W. Wong, and W. Y. Ching, Analytic solution of a two-dimensional hydrogen atom. I. Nonrelativistic theory, *Phys. Rev. A* **43**, 1186 (1991).
- [41] L. V. Keldysh, Coulomb interaction in thin semiconductor and semimetal films, *JETPL* **29**, 658 (1979).
- [42] K. He, N. Kumar, L. Zhao, Z. Wang, K. F. Mak, H. Zhao, and J. Shan, Tightly Bound Excitons in Monolayer WSe₂, *Phys. Rev. Lett.* **113**, 026803 (2014).
- [43] A. Chernikov, T. C. Berkelbach, H. M. Hill, A. Rigosi, Y. Li, B. Aslan, D. R. Reichman, M. S. Hybertsen, and T. F. Heinz, Exciton Binding Energy and Nonhydrogenic Rydberg Series in Monolayer WS₂, *Phys. Rev. Lett.* **113**, 076802 (2014).
- [44] Q. Hu, Z. Zhan, H. Cui, Y. Zhang, F. Jin, X. Zhao, M. Zhang, Z. Wang, Q. Zhang, K. Watanabe, T. Taniguchi, X. Cao, W.-M. Liu, F. Wu, S. Yuan, and Y. Xu, Observation of Rydberg moiré excitons, *Science* **380**, 1367 (2023).
- [45] V. Pareek, D. R. Bacon, X. Zhu, Y.-H. Chan, F. Bussolotti, N. S. Chan, J. P. Urquiza, K. Watanabe, T. Taniguchi, M. K. L. Man, J. Madéo, D. Y. Qiu, K. E. J. Goh, F. H. da Jornada, and K. M. Dani, Driving non-trivial quantum phases in conventional semiconductors with intense excitonic fields, *arXiv*: **2403**, 08725 (2024).
- [46] R. Mori, S. Ciocys, K. Takasan, P. Ai, K. Currier, T. Morimoto, J. E. Moore, and A. Lanzara, Spin-polarized spatially indirect excitons in a topological insulator, *Nature* **614**, 249 (2023).
- [47] E. J. Sie, J. W. McIver, Y.-H. Lee, L. Fu, J. Kong, and N. Gedik, Valley-selective optical Stark effect in monolayer WS₂, *Nat. Mater.* **14**, 290 (2015).
- [48] J.-Y. Shan, M. Ye, H. Chu, S. Lee, J.-G. Park, L. Balents, and D. Hsieh, Giant modulation of optical nonlinearity by Floquet engineering, *Nature* **600**, 235 (2021).

Supplemental Material for “Interaction Effects on the Electronic Floquet Spectra: Excitonic Effects”

Teng Xiao,¹ Tsan Huang,¹ Changhua Bao,¹ and Zhiyuan Sun^{1,2}

¹State Key Laboratory of Low-Dimensional Quantum Physics and Department of Physics, Tsinghua University, Beijing 100084, P. R. China

²Frontier Science Center for Quantum Information, Beijing 100084, P. R. China

(Dated: June 9, 2025)

CONTENTS

I. Non-equilibrium Green functions and the Dyson equation	1
II. Excitonic correction to the electron-photon vertex	2
A. Contribution from the scattering states	3
B. Effect of exciton-exciton nonlinear interactions	3
III. Discussion of the perturbation series	3
A. The Dyson resummation	4
B. The Taylor expansion of the self energy	4
IV. Excitonic correction to the retarded and lesser Green functions	5
A. Close to the exciton resonance	5
V. Connection to the conventional Floquet approach	6
VI. The ARPES signal	7
References	8

I. NON-EQUILIBRIUM GREEN FUNCTIONS AND THE DYSON EQUATION

Following Refs. [S1–S3], the fermion non-equilibrium Green functions are defined as

$$\hat{G}_{ab}(t, t') = -i \langle \psi_a(t) \bar{\psi}_b(t') \rangle = \begin{pmatrix} G^R(t, t') & G^K(t, t') \\ 0 & G^A(t, t') \end{pmatrix}, \quad (\text{S1})$$

where $a/b = 1/2$, $\psi_{1/2}(t) = \frac{1}{\sqrt{2}}(\psi^+(t) \pm \psi^-(t))$, $\bar{\psi}_{1/2}(t) = \frac{1}{\sqrt{2}}(\bar{\psi}^+(t) \mp \bar{\psi}^-(t))$, ψ^+/ψ^- is the field on the forward/backward part of the closed time contour, and $\langle \rangle$ means the path integral average so that the time-ordering symbol is not needed. For convenience of the readers, we also list the definition of the real-time Green functions from Eq. (S1) on the single time axis using the canonical formalism [S4]:

$$\begin{aligned} G^R(t, t') &= -i\theta(t - t') \left\langle [\psi(t), \psi^\dagger(t')]_\zeta \right\rangle = \theta(t - t') (G^>(t, t') - G^<(t, t')), \\ G^A(t, t') &= i\theta(t - t') \left\langle [\psi(t), \psi^\dagger(t')]_\zeta \right\rangle = -\theta(t - t') (G^>(t, t') - G^<(t, t')), \\ G^K(t, t') &= -i \left\langle [\psi(t), \psi^\dagger(t')]_{-\zeta} \right\rangle = G^>(t, t') + G^<(t, t') \end{aligned} \quad (\text{S2})$$

where $\langle \dots \rangle$ now means $\text{Tr}(\hat{\rho} \dots)$, $G^>(t, t') = -i \langle \psi(t) \psi^\dagger(t') \rangle$, $G^<(t, t') = -\zeta i \langle \psi^\dagger(t') \psi(t) \rangle$, and $\zeta = 1/-1$ for bosons/fermions.

The Dyson equation for the non-equilibrium Green function is

$$\hat{G} = \hat{G}_0 + \hat{G}_0 \hat{\Sigma} \hat{G}, \quad \hat{G} = \begin{pmatrix} G^R & G^K \\ 0 & G^A \end{pmatrix}, \quad \hat{\Sigma} = \begin{pmatrix} \Sigma^R & \Sigma^K \\ 0 & \Sigma^A \end{pmatrix} \quad (\text{S3})$$

where the products imply matrix multiplication and convolution in their time indices: $(\hat{\Sigma}\hat{G})(t_1, t_3) = \int dt_2 \hat{\Sigma}(t_1, t_2) \hat{G}(t_2, t_3)$. This is a natural result of re-summation as one performs perturbative expansion in the language of path integral on the Keldysh time contour [S3, S5]. Its solution in the matrix form is:

$$\hat{G} = (\hat{G}_0^{-1} - \hat{\Sigma})^{-1} = \begin{pmatrix} [G_0^R]^{-1} - \Sigma^R & [G_0^{-1}]^K - \Sigma^K \\ 0 & [G_0^A]^{-1} - \Sigma^A \end{pmatrix}^{-1}. \quad (\text{S4})$$

In terms of its retarded, advanced and Keldysh components, Eq. (S3) reads

$$\begin{cases} G^{R(A)} = G_0^{R(A)} + G_0^{R(A)} \Sigma^{R(A)} G^{R(A)} \\ G^K = G_0^K + G_0^R \Sigma^R G^K + G_0^R \Sigma^K G^A + G_0^K \Sigma^A G^A \end{cases} \quad (\text{S5})$$

and Eq. (S4) reads [S6]

$$\begin{cases} G^{R(A)} = (1 - G_0^{R(A)} \Sigma^{R(A)})^{-1} G_0^{R(A)} = \left([G_0^{R(A)}]^{-1} - \Sigma^{R(A)} \right)^{-1} \\ G^K = G^R (G_0^R)^{-1} G_0^K (G_0^A)^{-1} G^A + G^R \Sigma^K G^A = (1 + G^R \Sigma^R) G_0^K (1 + \Sigma^A G^A) + G^R \Sigma^K G^A \end{cases}. \quad (\text{S6})$$

For the two band model, the bare Green functions in the band basis are

$$G_{0,k}^{R/A}(\omega) = \begin{pmatrix} \frac{1}{\omega - \varepsilon_k^c \pm i\eta} & 0 \\ 0 & \frac{1}{\omega - \varepsilon_k^v \pm i\eta} \end{pmatrix}, \quad G_{0,k}^K(\omega) = -2\pi i [1 - 2n_F(\omega)] \begin{pmatrix} \delta(\omega - \varepsilon_k^c) & 0 \\ 0 & \delta(\omega - \varepsilon_k^v) \end{pmatrix} \quad (\text{S7})$$

where $n_F(\omega) = 1/(e^{(\omega - \mu)/T} + 1)$ is the equilibrium Fermi occupation function at temperature T .

II. EXCITONIC CORRECTION TO THE ELECTRON-PHOTON VERTEX

The first diagram in Fig. 1(b) of the main text corresponds to the second order term of A in the self energy:

$$\hat{\Sigma}_k(\omega) = \hat{\Gamma}_k(\omega, \omega + \omega_p) \hat{G}_{0,k}(\omega + \omega_p) \hat{\Gamma}_k(\omega + \omega_p, \omega) + (\omega_p \rightarrow -\omega_p) \quad (\text{S8})$$

where $\hat{\Gamma}_k$ is the light-matter coupling vertex, which may be re-normalized by electron-hole interactions. We next compute the vertex. As an example, the self-consistent equation for the interband vertex $\hat{\Gamma}_k^{cv}(\omega + \omega_p, \omega)$ shown in Fig. 1(c) of the main text is

$$\hat{\Gamma}_k^{cv}(\omega + \omega_p, \omega) = A_0 M_k \hat{\gamma}_c + \frac{i}{2} \left[\sum_{\omega', k'} V_{k-k'} \hat{\gamma}_c \hat{G}_{0,k'}^{cc}(\omega' + \omega_p) \Gamma_{k'}^{cv}(\omega' + \omega_p, \omega') \hat{G}_{0,k'}^{vv}(\omega') \hat{\gamma}_q + (\hat{\gamma}_c \leftrightarrow \hat{\gamma}_q) \right] \quad (\text{S9})$$

where $\hat{\gamma}_c = \begin{pmatrix} 1 & 0 \\ 0 & 1 \end{pmatrix}$ and $\hat{\gamma}_q = \begin{pmatrix} 0 & 1 \\ 1 & 0 \end{pmatrix}$ are the ‘classical’ and ‘quantum’ matrices in the Keldysh space [S3]. From the right hand side of Eq. (S9), one observes that the vertex is independent on ω so that $\hat{\Gamma}_k^{cv}(\omega + \omega_p, \omega) = \hat{\Gamma}_k^{cv}(\omega_p)$, i.e., it depends on the photon frequency only. Taking the trial solution $\hat{\Gamma}_k^{cv}(\omega_p) = \Gamma_k^{cv}(\omega_p) \hat{\gamma}_c$, Eq. (S9) is simplified to

$$\Gamma_k^{cv}(\omega_p) = A_0 M_k - \sum_{k'} V_{k-k'} \frac{1}{\omega_p + \varepsilon_{k'}^v - \varepsilon_{k'}^c + i0^+} \Gamma_{k'}^{cv}(\omega_p), \quad (\text{S10})$$

a typical Bethe–Salpeter equation. Before solving Eq. (S10), we define the eigen state problem between an electron and a hole:

$$(\varepsilon_k^c - \varepsilon_k^v - \omega_\lambda) \phi_\lambda(k) = \sum_{k'} V_{k-k'} \phi_\lambda(k') \quad (\text{S11})$$

where ω_λ and $\phi_\lambda(k)$ are the eigen energy and relative wave function of the two body problem [S7, S8]. The eigen states are classified into bound states ($\omega_\lambda < E_g$) meaning excitons, and scattering states ($\omega_\lambda > E_g$). Since $\phi_\lambda(k)$ forms a complete basis of functions, one may expand the vertex as $\Gamma_k^{cv}/(\omega + \varepsilon_k^v - \varepsilon_k^c + i0^+) = \sum_\lambda B_\lambda \phi_\lambda(k)$, which transforms Eq. (S10) into

$$\sum_\lambda B_\lambda \phi_\lambda(k) (\omega + \varepsilon_k^v - \varepsilon_k^c + i0^+) = A_0 M_k - \sum_{k', \lambda} V_{k-k'} B_\lambda \phi_\lambda(k') \quad (\text{S12})$$

Plugging Eq. (S11) into Eq. (S12) and taking into account the orthogonality properties of ϕ_λ yields the expansion coefficients:

$$B_\lambda = \frac{A_0}{\omega_p - \omega_\lambda + i0^+} \sum_k M_k \phi_\lambda^*(k). \quad (\text{S13})$$

Finally, one obtains the vertex as an expansion of all electron-hole two-body eigen states:

$$\Gamma_k^{cv}(\omega_p) = A_0 \sum_\lambda \left(\sum_{k'} M_{k'} \phi_\lambda^*(k') \right) \frac{\omega_p + \varepsilon_k^v - \varepsilon_k^c}{\omega_p - \omega_\lambda + i0^+} \phi_\lambda(k). \quad (\text{S14})$$

Note that ϕ_λ include both bound states (excitons) and scattering states. If an exciton has a finite lifetime, one may change 0^+ in Eq. (S14) to a phenomenological damping rate γ_λ . One observes that the vertex is resonantly enhanced if ω_p is close to a exciton resonance.

Noticing that $[\Gamma_k(\omega_p)]^\dagger = \Gamma_k(-\omega_p)$, the full vertex matrix reads

$$\Gamma_k(\omega_p) = \begin{pmatrix} \Gamma_k^{cc} & \Gamma_k^{cv}(\omega_p) \\ [\Gamma_k^{cv}(-\omega_p)]^* & \Gamma_k^{vv} \end{pmatrix}, \quad \Gamma_k(-\omega_p) = \begin{pmatrix} \Gamma_k^{cc} & \Gamma_k^{cv}(-\omega_p) \\ [\Gamma_k^{cv}(\omega_p)]^* & \Gamma_k^{vv} \end{pmatrix}, \quad (\text{S15})$$

where $\Gamma_k^{cc} = A_0 k/m_c$ and $\Gamma_k^{vv} = -A_0 k/m_v$.

A. Contribution from the scattering states

In the numerical results shown in the main text, we focus on the simple case of a constant interband optical matrix element $M_k = M$ so that the exciton-corrected vertex is simplified to

$$\begin{aligned} \Gamma_k^{cv}(\omega_p) &= A_0 M (\omega_p + \varepsilon_k^v - \varepsilon_k^c) \sum_\lambda \frac{\phi_\lambda^*(r=0) \phi_\lambda(k)}{\omega_p - \omega_\lambda + i\gamma_\lambda} \\ &= A_0 M (\omega_p + \varepsilon_k^v - \varepsilon_k^c) \left(\sum_{\lambda \in \text{bound}} \frac{\phi_\lambda^*(r=0) \phi_\lambda(k)}{\omega_p - \omega_\lambda + i\gamma_\lambda} + \sum_{\lambda \in \text{scatter}} \frac{\phi_\lambda^*(r=0) \phi_\lambda(k)}{\omega_p - \omega_\lambda + i\gamma_\lambda} \right) \\ &= \Gamma_{k,\text{bound}}^{cv}(\omega_p) + \Gamma_{k,\text{scatter}}^{cv}(\omega_p) \end{aligned} \quad (\text{S16})$$

which contains bound state and scattering state contributions. The bound state wavefunction and the excitonic energy is known in analytical forms. We perform the summation over λ_{bound} to a cutoff of 10 to get a converged result.

The summation over the scattering states with a continuous index is hard to perform, which we replace by an approximation formula. Motivated by the free limit, we assume the scattering state wave function with energy $\omega_{\lambda_{\text{scatter}}}$ is a linear combination of free electron-hole states with the relative momenta at all directions but with a fixed magnitude $|\mathbf{k}| = k_E$ satisfying $\omega_{\lambda_{\text{scatter}}} = k_E^2/m + E_g$ where $2/m = 1/m_c + 1/m_v$.

From the relation $\langle k|r=0 \rangle = 1$, we have $\sum_\lambda \phi_\lambda(k) \phi_\lambda^*(r=0) = \sum_{\lambda \in \text{bound}} \phi_\lambda(k) \phi_\lambda^*(r=0) + \sum_{\lambda \in \text{scatter}} \phi_\lambda(k) \phi_\lambda^*(r=0) = 1$. Therefore, assuming $\gamma_\lambda = \gamma$, the scattering state contribution could be expressed in terms of bound states as

$$\begin{aligned} \Gamma_{k,\text{scatter}}^{cv}(\omega_p) &\approx A_0 M (\omega_p + \varepsilon_k^v - \varepsilon_k^c) \frac{\sum_{\lambda \in \text{scatter}} \phi_\lambda^*(r=0) \phi_\lambda(k)}{\omega_p - (k^2/m + E_g) + i\gamma_\lambda} \\ &= A_0 M (\omega_p + \varepsilon_k^v - \varepsilon_k^c) \frac{1 - \sum_{\lambda \in \text{bound}} \phi_\lambda^*(r=0) \phi_\lambda(k)}{\omega_p - (k^2/m + E_g) + i\gamma_\lambda}. \end{aligned}$$

B. Effect of exciton-exciton nonlinear interactions

By making a comparison to the description of exciton-exciton interactions in terms of the Hubbard-Stratonovich field [S9], the effect of exciton-exciton interactions are included by the diagrams shown in Fig. S1. We leave the evaluation of these diagrams for future research.

III. DISCUSSION OF THE PERTURBATION SERIES

In this section, we discuss the convergence property of the perturbation series for the case of single color pump with no phase randomness. Same as the main text, we focus on the time averaged Green function $G(\omega) = \int_0^T G(\omega, t_0) dt_0 / T$ only.

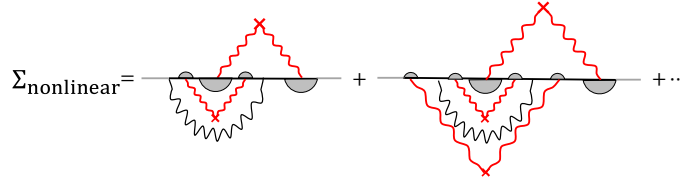


FIG. S1. The self energy diagrams containing the effects of the two-exciton interactions, which lie in the series shown in Fig. 1b in the main text.

A. The Dyson resummation

The goal of the computation is the Green function. Dyson re-summation states that one may define the self energy (1PI diagrams defined in the main text) in Eq. (S3) and perform Taylor expansion of the self energy, which yields the Green function through the Dyson equation. For the excitonic effects, there is a small parameter that justifies this re-summation when the pump frequency is close to the exciton energy, as discussed in the main text. For example, compared to the reducible diagram $G_0 \Sigma G_0 \Sigma G_0$ included by the Dyson's equation with the leading order self energy, the second diagram in Fig. 1b of the main text is smaller by the ratio

$$a_1 \sim \frac{\Gamma^{cv}(-\omega_p) G_0(\omega + 2\omega_p) \Gamma^{vc}(\omega_p)}{\Gamma^{cv}(\omega_p) G_0(\omega) \Gamma^{vc}(-\omega_p)} \approx \left| \frac{(\omega_p + E_g)(\omega_p - \omega_\lambda)}{(\omega_p + \omega_\lambda)(\omega_p - E_g)} \right|^2 \ll 1. \quad (\text{S17})$$

B. The Taylor expansion of the self energy

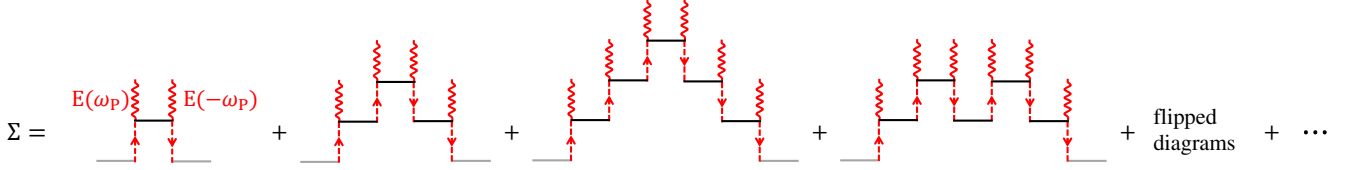


FIG. S2. The diagrammatic expansion of the self-energy Σ . The red wavy lines represent the pump light, which are connected to the steps shown by red dashed lines representing the rising and lowering of frequencies by ω_p . The gray lines represent external electron legs and should not be included when computing this self energy. The height of the self energy could be defined as the maximum height of the ladder. For example, the heights of the diagrams are 1, 2, 3, 2 from left to right in the figure.

The Taylor expansion $\Sigma = \sum_n c_{2n} E^{2n} = \sum_n c'_{2n} a_2^{2n}$ of the self energy itself could be viewed as an expansion in a dimensionless small parameter proportional to the driving field, which is about $a_2 \sim A_0 M / \omega_p$ for large n as long as $n\omega_p$ is much larger than the relevant electronic band width. The Taylor expansion series could be grouped diagrammatically in Fig. S2. At order E_p^{2n} for $n \geq 1$, the number of distinct self energies equals twice the $n - 1$ Catalan number: $N_p^{2n} = \frac{2}{n} \binom{2n-2}{n-1}$.

The value of each self energy could be read from the diagram directly. For the convenience of readers not comfortable with diagrams, we also show the symbolic derivations. Assuming that $\hat{G}_0(t, t')$ is the equilibrium green function and $\hat{V}(t)$ is the time-periodic pumping term, the full Green function may be written as the 'grand Dyson equation'

$$\hat{G}(t, t') = \hat{G}_0(t, t') + \int d\tau \hat{G}_0(t, \tau) \hat{V}(\tau) \hat{G}(\tau, t'). \quad (\text{S18})$$

Iterating it, the result at every order of V can be obtained. As in the main text, we consider only the frequency-conserved Green function as the frequency-non-conserved ones would vanish after time-average and could hardly be resolved in typical ultra-fast experiments. Therefore, only even orders of V are needed. Expanding Eq. (S18) to fourth order of V yields

$$\begin{aligned} \hat{G}(\omega) = & \hat{G}_0(\omega) + \hat{G}_0(\omega) \left[\int d\omega_p \hat{V}(-\omega_p) \hat{G}_0(\omega + \omega_p) \hat{V}(\omega_p) \right] \hat{G}_0(\omega) + \\ & \hat{G}_0(\omega) \left\{ \left[\int d\omega_p \hat{V}(-\omega_p) \hat{G}_0(\omega + \omega_p) \hat{V}(\omega_p) \right] \hat{G}_0(\omega) \left[\int d\bar{\omega}_p \hat{V}(-\bar{\omega}_p) \hat{G}_0(\omega + \bar{\omega}_p) \hat{V}(\bar{\omega}_p) \right] + \right. \\ & \left. \left[\int d\omega_p \hat{V}(-\omega_p) \hat{G}_0(\omega + \omega_p) \hat{V}(-\omega_p) \hat{G}_0(\omega + 2\omega_p) \hat{V}(\omega_p) \hat{G}_0(\omega + \omega_p) \hat{V}(\omega_p) \right] \right\} \hat{G}_0(\omega). \end{aligned} \quad (\text{S19})$$

Comparing to the Dyson's equation for the equal-frequency Green function in Eq. (S3), the self-energy at order V^2 (first diagram in Fig. S2) is therefore

$$\hat{\Sigma}^{(2)} = \int d\omega_p \hat{V}(-\omega_p) \hat{G}_0(\omega + \omega_p) \hat{V}(\omega_p) \quad (\text{S20})$$

and its flipped version ($\omega_p \rightarrow -\omega_p$). The self-energy at order V^4 (second diagram in Fig. S2)

$$\hat{\Sigma}^{(4)} = \int d\omega_p \hat{V}(-\omega_p) \hat{G}_0(\omega + \omega_p) \hat{V}(-\omega_p) \hat{G}_0(\omega + 2\omega_p) \hat{V}(\omega_p) \hat{G}_0(\omega + \omega_p) \hat{V}(\omega_p) \quad (\text{S21})$$

and its flipped version.

IV. EXCITONIC CORRECTION TO THE RETARDED AND LESSER GREEN FUNCTIONS

The retarded Green function is found from Eq. (S6) with the retarded self energy

$$\Sigma^R(\omega) = \Gamma_k(-\omega_p) G_{0,k}^R(\omega + \omega_p) \Gamma_k(\omega_p) + (\omega_p \rightarrow -\omega_p). \quad (\text{S22})$$

being the first diagram in Fig. S2 (the lowest order in the pump field). The retarded self energy is a two-by-two matrix in the band basis with the matrix elements

$$\begin{aligned} \Sigma_{cc}^R &= |\Gamma_k^{cc}|^2 G_{0,cc}^R(\omega + \omega_p) + |\Gamma_k^{cv}(-\omega_p)|^2 G_{0,vv}^R(\omega + \omega_p) + (\omega_p \rightarrow -\omega_p), \\ \Sigma_{cv}^R &= \Gamma_k^{cc} \Gamma_k^{cv}(\omega_p) G_{0,cc}^R(\omega + \omega_p) + \Gamma_k^{cv}(-\omega_p) \Gamma_k^{vv} G_{0,vv}^R(\omega + \omega_p) + (\omega_p \rightarrow -\omega_p), \\ \Sigma_{vc}^R &= [\Gamma_k^{cv}(\omega_p)]^* \Gamma_k^{cc} G_{0,cc}^R(\omega + \omega_p) + \Gamma_k^{vv} [\Gamma_k^{cv}(-\omega_p)]^* G_{0,vv}^R(\omega + \omega_p) + (\omega_p \rightarrow -\omega_p), \\ \Sigma_{vv}^R &= |\Gamma_k^{vv}|^2 G_{0,vv}^R(\omega + \omega_p) + |\Gamma_k^{cv}(\omega_p)|^2 G_{0,cc}^R(\omega + \omega_p) + (\omega_p \rightarrow -\omega_p). \end{aligned} \quad (\text{S23})$$

The lesser Green function $G^< = (G^K + G^A - G^R)/2$ is found from Eq. (S6) as

$$\begin{aligned} G^< &= G^R [G_0^R]^{-1} G_0^< [G_0^A]^{-1} G^A + G^R \Sigma^< G^A \\ &= \left(\begin{array}{cc} G_{cv}^R [G_{0,vv}^R]^{-1} G_{0,vv}^< [G_{0,vv}^A]^{-1} G_{vc}^A & G_{cv}^R [G_{0,vv}^R]^{-1} G_{0,vv}^< [G_{0,vv}^A]^{-1} G_{vv}^A \\ G_{vv}^R [G_{0,vv}^R]^{-1} G_{0,vv}^< [G_{0,vv}^A]^{-1} G_{vc}^A & G_{vv}^R [G_{0,vv}^R]^{-1} G_{0,vv}^< [G_{0,vv}^A]^{-1} G_{vv}^A \end{array} \right) + \\ &\quad \left(\begin{array}{cc} G_{cc}^R \Sigma_{cc}^< G_{cc}^A + G_{cv}^R \Sigma_{vc}^< G_{cc}^A + G_{cc}^R \Sigma_{cv}^< G_{vc}^A + G_{cv}^R \Sigma_{vv}^< G_{vc}^A & G_{cc}^R \Sigma_{cc}^< G_{cv}^A + G_{cv}^R \Sigma_{vc}^< G_{cv}^A + G_{cc}^R \Sigma_{cv}^< G_{vv}^A + G_{cv}^R \Sigma_{vv}^< G_{vv}^A \\ G_{vc}^R \Sigma_{cc}^< G_{cc}^A + G_{vv}^R \Sigma_{vc}^< G_{cc}^A + G_{vc}^R \Sigma_{cv}^< G_{vc}^A + G_{vv}^R \Sigma_{vv}^< G_{vc}^A & G_{vc}^R \Sigma_{cc}^< G_{cv}^A + G_{vv}^R \Sigma_{vc}^< G_{cv}^A + G_{vc}^R \Sigma_{cv}^< G_{vv}^A + G_{vv}^R \Sigma_{vv}^< G_{vv}^A \end{array} \right), \end{aligned} \quad (\text{S24})$$

where

$$\begin{aligned} \Sigma^< &= \left(\begin{array}{cc} |\Gamma_k^{cv}(-\omega_p)|^2 G_{0,vv}^<(\omega + \omega_p) & \Gamma_k^{cv}(-\omega_p) \Gamma_k^{vv} G_{0,vv}^<(\omega + \omega_p) \\ \Gamma_k^{vv} [\Gamma_k^{cv}(-\omega_p)]^* G_{0,vv}^<(\omega + \omega_p) & |\Gamma_k^{vv}|^2 G_{0,vv}^<(\omega + \omega_p) \end{array} \right) + \\ &\quad \left(\begin{array}{cc} |\Gamma_k^{cv}(\omega_p)|^2 G_{0,vv}^<(\omega - \omega_p) & \Gamma_k^{cv}(\omega_p) \Gamma_k^{vv} G_{0,vv}^<(\omega - \omega_p) \\ \Gamma_k^{vv} [\Gamma_k^{cv}(\omega_p)]^* G_{0,vv}^<(\omega - \omega_p) & |\Gamma_k^{vv}|^2 G_{0,vv}^<(\omega - \omega_p) \end{array} \right) \end{aligned} \quad (\text{S25})$$

is the lesser self energy.

A. Close to the exciton resonance

Close to the exciton resonances, the Green functions can be simplified by neglecting the terms containing Γ_k^{cc} and Γ_k^{vv} which do not contain the exciton contributions. In this limit, the self energy in Eq. (S22) has only diagonal components, see Eq. (S23). If one further neglects the far-from-resonant terms such as $\Gamma_k^{cv}(-\omega_p)$, the retarded self energy is simplified to

$$\Sigma^R = |\Delta_k|^2 \begin{pmatrix} G_{0,vv}^R(\omega - \omega_p) & 0 \\ 0 & G_{0,cc}^R(\omega + \omega_p) \end{pmatrix}, \quad (\text{S26})$$

where $\Delta_k = \Gamma_k^{cv}(\omega_p)$ is the exciton-modified vertex in Eq. (S14). From Eq. (S6), the retarded Green functions are found as

$$G_{cc}^R = \frac{1}{[G_{0,cc}^R(\omega)]^{-1} - |\Delta_k|^2 G_{0,vv}^R(\omega - \omega_p)} = \frac{\omega - \omega_p - \varepsilon_k^v + i0^+}{(\omega - E_1^c)(\omega - E_2^c) + i0^+(2\omega - E_1^c - E_2^c)},$$

$$G_{vv}^R = \frac{1}{[G_{0,vv}^R(\omega)]^{-1} - |\Delta_k|^2 G_{0,cc}^R(\omega + \omega_p)} = \frac{\omega + \omega_p - \varepsilon_k^c + i0^+}{(\omega - E_1^v)(\omega - E_2^v) + i0^+(2\omega - E_1^v - E_2^v)},$$

where

$$E_{1/2}^c = \frac{\varepsilon_k^c + \varepsilon_k^v + \omega_p \pm \sqrt{(\varepsilon_k^c - \varepsilon_k^v - \omega_p)^2 + 4|\Delta_k|^2}}{2}, \quad E_{1/2}^v = \frac{\varepsilon_k^v + \varepsilon_k^c - \omega_p \pm \sqrt{(\varepsilon_k^v - \varepsilon_k^c + \omega_p)^2 + 4|\Delta_k|^2}}{2}. \quad (\text{S27})$$

The advanced Green functions are related to the retarded ones by $G^A = G^{R*}$.

The lesser self energy from Eq. (S25) is

$$\Sigma^< = |\Delta_k|^2 \begin{pmatrix} G_{0,vv}^<(\omega - \omega_p) & 0 \\ 0 & 0 \end{pmatrix} \quad (\text{S28})$$

considering the property of the ground state $(\hat{c}_k |0\rangle = \hat{v}_k^\dagger |0\rangle = 0)$. From Eq. (S24), we obtain the lesser Green functions as

$$G_{cc}^< = G_{cc}^R \Sigma_{cc}^< G_{cc}^A = |\Delta_k|^2 |G_{cc}^R|^2 G_{0,vv}^<(\omega - \omega_p) = 2\pi i \frac{|\Delta_k|^2}{|E_1^c - E_2^c|^2} (\delta(\omega - E_1^c) + \delta(\omega - E_2^c))$$

$$= 2\pi i \frac{|\Delta_k|^2}{(\varepsilon_k^c - \omega_p - \varepsilon_k^v)^2 + 4|\Delta_k|^2} (\delta(\omega - E_1^c) + \delta(\omega - E_2^c)),$$

$$G_{vv}^< = G_{vv}^R [G_{0,vv}^R]^{-1} G_{0,vv}^< [G_{0,vv}^A]^{-1} G_{vv}^A = |G_{vv}^R|^2 |G_{0,vv}^R|^{-1} G_{0,vv}^<(\omega) = 2\pi i \frac{(\omega + \omega_p - \varepsilon_k^c)^2}{|E_1^v - E_2^v|^2} (\delta(\omega - E_1^v) + \delta(\omega - E_2^v))$$

$$= 2\pi i \frac{(\omega + \omega_p - \varepsilon_k^c)^2}{(\omega_p + \varepsilon_k^v - \varepsilon_k^c)^2 + 4|\Delta_k|^2} (\delta(\omega - E_1^v) + \delta(\omega - E_2^v)). \quad (\text{S29})$$

V. CONNECTION TO THE CONVENTIONAL FLOQUET APPROACH

If one neglects the electron-hole interaction H_{ee} in H of Eq. 3 in the main text, the corresponding Floquet matrix F using the conventional Floquet approach is

$$F = \begin{pmatrix} \ddots & & & & \\ V_f & H_0 - \omega_p & V_f & & \\ & V_f & H_0 & V_f & \\ & & V_f & H_0 + \omega_p & V_f \\ & & & & \ddots \end{pmatrix}, \quad (\text{S30})$$

where $H_0 = \begin{pmatrix} \varepsilon_k^c & \\ & \varepsilon_k^v \end{pmatrix}$, and $V_f = A \begin{pmatrix} k/m_c & M_k \\ M_k & -k/m_v \end{pmatrix}$ is the light matter coupling vertex. With the interaction modified vertex Γ_k derived in Sec. II, one may simply replace the bare coupling V_f by the interaction corrected vertex, so that the Floquet matrix F_c becomes

$$F_c = \begin{pmatrix} \ddots & & & & \\ \Gamma_k(-\omega_p) & H_0 - \omega_p & \Gamma_k(\omega_p) & & \\ & \Gamma_k(-\omega_p) & H_0 & \Gamma_k(\omega_p) & \\ & & \Gamma_k(-\omega_p) & H_0 + \omega_p & \Gamma_k(\omega_p) \\ & & & & \ddots \end{pmatrix}. \quad (\text{S31})$$

By diagonalizing this Floquet matrix F_c , one obtains its eigenvalues as the quasi-energies, resulting in the same interaction-corrected Floquet bands as those from the Green function method. However, the exact correspondence is complicated by a finite

frequency cutoff. For a cutoff frequency index $\pm\omega_p$ of the Floquet matrix F_c , the quasi-energies correspond to keeping the $O(E_p^2)$ self-energy used in the main text. For a cutoff frequency $\pm n\omega_p$, the quasi energies from the Floquet matrix correspond to summing all the self energies whose heights lie within $\pm n$ in Fig. S2. However, it no longer corresponds to a certain order of the self energy in the pump field.

In the Green function approach, one may define $\hat{\Sigma}_{(n)}^+$ as the sum of all self energy diagrams whose heights are positive but not higher than $+n$. Similarly, the Green function $\hat{G}_{(n)}^+ = [\hat{G}_0^{-1} - \hat{\Sigma}_{(n)}^+]^{-1}$ contains all the diagrams whose heights are positive but not higher than $+n$. They satisfy the recursive relation:

$$\hat{\Sigma}_{(n+1)}^+(\omega) = \hat{\Gamma}(-\omega_p)\hat{G}_{(n)}^+(\omega + \omega_p)\hat{\Gamma}(\omega_p). \quad (\text{S32})$$

Numerically, the self energy could be computed height by height in this way. The the downward self-energy $\hat{\Sigma}_{(-n)}^-$ may be obtained in a similar way. The sum $\hat{\Sigma}_{(n)}^+ + \hat{\Sigma}_{(-n)}^-$ thus corresponds to all the self energies whose heights lie within $\pm n$.

VI. THE ARPES SIGNAL

The probe part of the Hamiltonian for ARPES is

$$H_f = \sum_k \varepsilon_k^f f_k^\dagger f_k, \quad H_b = A_b(t) \sum_k \left(M_{fc}(k) f_k^\dagger c_k + M_{fv}(k) f_k^\dagger v_k + \text{h.c.} \right) \quad (\text{S33})$$

where $\varepsilon_k^f = k^2/2m_e$ is the kinetic energy of the free electron with f_k being its annihilation operator, $A_b(t) = A_b e^{-i\omega_b t} + \text{c.c.}$ is the vector potential of the probe field, M_{fc} (M_{fv}) is the optical matrix element between free electrons f and the electrons in conduction (valence) band. The time-accumulated ARPES intensity is

$$I_k^{\text{sum}} = \int_{t_0}^{t_f} dt \frac{\partial}{\partial t} \rho_k^f = \int_{t_0}^{t_f} dt I_k, \quad (\text{S34})$$

where I_k is the ARPES intensity, $\rho_k^f = \langle f_k^\dagger f_k \rangle = -iG_{ff}^<(t, t)$ and $G_{ff}^<$ is the lesser Green function of the free space electrons collected by the detector. To eliminate the time derivative, we use the Heisenberg equation of motion $i\partial_t A = [A, H]$:

$$I_k = \frac{\partial}{\partial t} \rho_k^f = -i \frac{\partial}{\partial t} G_{ff}^<(t, t) = 2 \text{Re} \left(\sum_{\alpha=\{c,v\}} M_{\alpha f}(k) A_b(t) G_{f\alpha}^<(t, t) \right) \quad (\text{S35})$$

where $G_{f\alpha}^<(t, t') = i \langle \alpha_k^\dagger(t') f_k(t) \rangle$. For the ground state $|0\rangle$ satisfying $f_k |0\rangle = c_k |0\rangle = v_k^\dagger |0\rangle = 0$, the bare lesser, retarded and advanced Green functions are

$$\begin{aligned} G_0^<(t, t') &= \text{diag} \left(G_{0,ff}^<(t, t'), G_{0,cc}^<(t, t'), G_{0,vv}^<(t, t') \right) = \text{diag} \left(0, 0, i e^{i\varepsilon_k^v(t'-t)} \right), \\ G_0^R(t, t') &= \text{diag} \left(G_{0,ff}^R(t, t'), G_{0,cc}^R(t, t'), G_{0,vv}^R(t, t') \right), \\ G_0^A(t, t') &= \text{diag} \left(G_{0,ff}^A(t, t'), G_{0,cc}^A(t, t'), G_{0,vv}^A(t, t') \right), \end{aligned} \quad (\text{S36})$$

where $G_{0,ff/cc/vv}^R(t, t') = -\theta(t - t') i e^{-i\varepsilon_k^{f/c/v}(t-t')}$ and $G_{0,ff/cc/vv}^A(t, t') = \theta(t' - t) i e^{i\varepsilon_k^{f/c/v}(t'-t)}$. Using the Langreth rules to the grand Dyson equation, we obtain

$$G_{f\alpha}^<(t, t') = \sum_{\beta=\{c,v\}} \int_{-\infty}^{+\infty} d\bar{t} G_{0,ff}^R(t, \bar{t}) M_{f\beta}(k) A_b(\bar{t}) G_{\beta\alpha}^<(\bar{t}, t'). \quad (\text{S37})$$

to the first order in the probe field. From (S35), the ARPES intensity is related to the lesser Green function of electrons inside the material [S10]:

$$\begin{aligned} I_k &= 2 \text{Re} \left(\sum_{\alpha,\beta} M_{\beta f}(k) A_b(t) \int_{-\infty}^{+\infty} d\bar{t} G_{0,ff}^R(t, \bar{t}) M_{f\alpha}(k) A_b(\bar{t}) G_{\alpha\beta}^<(\bar{t}, t) \right) \\ &= -i |A_b|^2 \sum_{\alpha,\beta} M_{f\alpha}(k) M_{\beta f}(k) G_{\alpha\beta}^<(\varepsilon_k^f \pm \omega_b). \end{aligned} \quad (\text{S38})$$

Here $G^<$ is the corrected Green function that contains the effect of the interaction and the pumping field. For more realistic cases, the probe field is a pulse $A_b(t) = A_b s_b(t) e^{-i\omega_b t} + \text{c.c.}$ where $s_b(t) = \exp(-\frac{(t-t_d)^2}{2\sigma^2})$. The time-accumulated ARPES intensity is further broadened to

$$I_k^{\text{sum}} = \int_{t_0}^{t_f} dt I_k = -i2\pi\sigma^2 |A_b|^2 \sum_{\alpha,\beta} M_{f\alpha}(k) M_{\beta f}(k) \int \frac{d\omega}{2\pi} e^{-\sigma^2(\epsilon_k^f \pm \omega_b - \omega)^2} G_{\alpha\beta}^<(\omega). \quad (\text{S39})$$

where we take $t_f \rightarrow +\infty$ and $t_0 \rightarrow -\infty$. However, we take $\sigma = \infty$ for the numerical plots in the main text, meaning single colored probe light.

-
- [S1] L. V. Keldysh, Diagram technique for nonequilibrium processes, *Zh. Eksp. Teor. Fiz.* **47**, 1515 (1964).
[S2] A. I. Larkin and Y. N. Ovchinnikov, Nonlinear conductivity of superconductors in the mixed state, *Sov. Phys. JETP* **41**, 960 (1975).
[S3] A. Kamenev, *Field Theory of Non-Equilibrium Systems* (Cambridge University Press, Cambridge, England, 2011).
[S4] J. Rammer, *Quantum Field Theory of Non-equilibrium States* (Cambridge University Press, Cambridge, England, 2007).
[S5] A. Altland and B. Simons, *Condensed Matter Field Theory*, 3rd ed. (Cambridge University Press, Cambridge, England, 2023).
[S6] H. Haug and A.-P. Jauho, *Quantum Kinetics in Transport and Optics of Semiconductors* (Springer Berlin, Heidelberg, 2008).
[S7] M. Shinada and S. Sugano, Interband Optical Transitions in Extremely Anisotropic Semiconductors. I. Bound and Unbound Exciton Absorption, *J. Phys. Soc. Jpn.* **21**, 1936 (1966).
[S8] X. L. Yang, S. H. Guo, F. T. Chan, K. W. Wong, and W. Y. Ching, Analytic solution of a two-dimensional hydrogen atom. I. Nonrelativistic theory, *Phys. Rev. A* **43**, 1186 (1991).
[S9] Z. Sun, Y. Murakami, F. Xuan, T. Kaneko, D. Golež, and A. J. Millis, Dynamical Exciton Condensates in Biased Electron-Hole Bilayers, *Phys. Rev. Lett.* **133**, 217002 (2024).
[S10] C. Bao, M. Schüller, T. Xiao, F. Wang, H. Zhong, T. Lin, X. Cai, T. Sheng, X. Tang, H. Zhang, P. Yu, Z. Sun, W. Duan, and S. Zhou, Manipulating the symmetry of photon-dressed electronic states, *Nat. Commun.* **15**, 10535 (2024).